Ocular Counterroll Modulates the Preferred Direction of Saccade-Related Pontine Burst Neurons in the Monkey

HANSJÖRG SCHERBERGER,[1] JAN-HARRY CABUNGCAL,[1] KLAUS HEPP,[2] YASUO SUZUKI,[1,3] DOMINIK STRAUMANN,[1] AND VOLKER HENN[1,✠]

[1]*Neurology Department, Zürich University Hospital, CH-8091 Zürich;* [2]*Institute of Theoretical Physics, Eidgenössisch-Technische Hochschule, CH-8093 Zürich, Switzerland; and* [3]*Department of Ophthalmology, Sapporo Medical University, 060-8543 Sapporo, Japan*

Received 4 April 2000; accepted in final form 3 May 2001

Scherberger, Hansjörg, Jan-Harry Cabungcal, Klaus Hepp, Yasuo Suzuki, Dominik Straumann, and Volker Henn. Ocular counterroll modulates the preferred direction of saccade-related pontine burst neurons in the monkey. *J Neurophysiol* 86: 935–949, 2001. Saccade-related burst neurons in the paramedian pontine reticular formation (PPRF) of the head-restrained monkey provide a phasic velocity signal to extraocular motoneurons for the generation of rapid eye movements. In the superior colliculus (SC), which directly projects to the PPRF, the motor command for conjugate saccades with the head restrained in a roll position is represented in a reference frame in between oculocentric and space-fixed coordinates with a clear bias toward gravity. Here we studied the preferred direction of premotor burst neurons in the PPRF during static head roll to characterize their frame of reference with respect to head and eye position. In 59 neurons (short-lead, burst-tonic, and long-lead burst neurons), we found that the preferred direction of eye displacement of these neurons changed, relative to head-fixed landmarks, in the horizontal-vertical plane during static head roll. For the short-lead burst neurons and the burst-tonic group, the change was about one-fourth of the amount of ocular counterroll (OCR) and significantly different from a head-centered representation. In the long-lead burst neurons, the rotation of the preferred direction showed a larger trend of about one-half of OCR. During microelectrical stimulation of the PPRF (9 sites in 2 monkeys), the elicited eye movements rotated with about one-half the amount of OCR. In a simple pulley model of the oculomotor plant, the noncraniocentric reference frame of the PPRF output neurons could be reproduced for recently measured pulley positions, if the pulleys were assumed to rotate as a function of OCR with a gain of 0.5. We conclude that the saccadic displacement signal is transformed from a representation in the SC with a clear bias to gravity to a representation in the PPRF that is closely craniocentric, but rotates with OCR, consistent with current concepts of the oculomotor plant.

INTRODUCTION

Premotor saccadic burst neurons provide a velocity signal for the extra-ocular motoneurons to generate rapid eye movements in the head-restrained monkey (Büttner-Ennever and Henn 1976; Fuchs and Luschei 1970; Henn and Cohen 1976). In the brain stem, burst neurons of the paramedian pontine reticular formation (PPRF) code for horizontal components of eye movements (Cohen et al. 1968; Hepp and Henn 1983; Keller 1974; Luschei and Fuchs 1972; Robinson 1970), while neural coding of vertical and torsional eye movement components has been demonstrated in the rostral interstitial nucleus of the medial longitudinal fasciculus (riMLF) (Büttner et al. 1977; Büttner-Ennever and Büttner 1978; King and Fuchs 1979; Vilis et al. 1989). For saccade generation, the PPRF receives a major direct input from the superior colliculus (SC), where saccade-related burst neurons represent eye displacements in a two-dimensional motor map (Mays and Sparks 1980; Raybourn and Keller 1977; Robinson 1972; Van Opstal et al. 1991; for a review see Sparks 1999).

Recently, it was shown that the preferred direction of saccade-related burst neurons in the SC is modulated by head roll with respect to gravity (Frens et al. 1998). The preferred direction, defined individually for each neuron as the unique saccade direction associated with the most vigorous burst activity, stayed in the horizontal-vertical plane and rotated within that plane by an angle that exceeded the amount of ocular counterroll (OCR). It was concluded that SC burst neurons code the saccade vector in an intermediate reference frame that, although closely oculocentric, has a clear bias to gravity. In this study, we posed the same question for the saccadic premotor burst neurons in the PPRF: we asked whether the preferred direction of the three different types of presaccadic burst neurons, i.e., short-lead burst neurons (SBN), burst-tonic neurons (BTN), and long-lead burst neurons (LBN), (see, e.g., Hepp and Henn 1983), vary under head roll, and if so, in what reference frame they operate.

The exact mathematical relation between the horizontal-vertical direction of gaze and the amount of ocular torsion with the head stationary was first given by J. B. Listing (Helmholtz 1867; Ruete 1855). Any eye position, if described by a single rotation from primary position, lies in a plane that is perpendicular to the direction of gaze in primary position. This plane is called Listing's plane, and the corresponding coordinates of eye positions having their origin in primary position we will name Listing's coordinates. This law, Listing's law, holds true not only for eye positions during static fixations, but also, to a good approximation, during smooth pursuit and saccadic eye movements (Ferman et al. 1987; Haslwanter et al. 1991; Strau-

✠ Deceased 3 December 1997.

Present address and address for reprint requests: H. Scherberger, Div. of Biology, Mail Code 216-76, California Institute of Technology, Pasadena, CA 91125 (E-mail: hans@vis.caltech.edu).

The costs of publication of this article were defrayed in part by the payment of page charges. The article must therefore be hereby marked "*advertisement*" in accordance with 18 U.S.C. Section 1734 solely to indicate this fact.

mann et al. 1996; Tweed and Vilis 1990). When the head is statically rolled, the amount of eye torsion varies due to OCR. OCR is a static vestibuloocular reflex elicited by otolith input with a gain of about 0.1–0.2, good stability, and no habituation (Haslwanter et al. 1992; Suzuki et al. 1997). In Listing's coordinates, observed three-dimensional eye positions are particularly simple to describe: eye torsion is constant for each static head roll position (see, e.g., Hepp et al. 1997).

The actual axis around which the eye rotates during a saccade is not identical with the axis of the eye displacement (which is confined in Listing's plane), but is tilted, for geometrical reasons, out of Listing's plane by half the amount of the eye position's eccentricity according to the so-called "half-angle rule" (Tweed and Vilis 1990). This difference between the eye position displacement (displacement vector, d-vector) and the actual eye rotation (rotation vector, r-vector) touches the heart of the coding problem. The question arose, whether the premotor burst neurons encode the actual three-dimensional eye rotation, as predicted by a mathematically correct extension of the earlier one-dimensional Robinson (1975) model (Tweed and Vilis 1987), or whether a commutative signal is encoded instead, like the eye position displacement (Crawford 1994; Schnabolk and Raphan 1994), which would render the eye velocity-to-position integration, for instance, particularly simple. As an important consequence, an eye displacement (d-vector) coding scheme of the premotor burst neurons would imply that Listing's law is implemented downstream, e.g., at the level of the motoneurons or the oculomotor plant, while an eye rotation (r-vector) scheme would require Listing's law to be implemented upstream to the burst neurons.

In our lab, a recent study has found that the neural saccade activity in reticular burst neurons correlates better with the three-dimensional eye displacement (d-vector) than with the (also 3-dimensional) eye rotation (r-vector) coding scheme (Hepp et al. 1999). In this paper, we will consider both coding schemes as possible alternatives for the formulation of our hypotheses and the discussion of our results. For consistent description of our experimental results, however, we will express saccadic eye movements in terms of eye displacement (d-vector) only, and with respect to a head-centered reference frame (Fig. 1*A*).

For each coding scheme assumption, two anatomically different frames of reference can be considered (Fig. 1*B*). Let us first assume that the premotor burst neurons encode in an eye displacement scheme:

I. If the displacement coding is in a *craniocentric reference frame,* the preferred direction of eye displacement (d-vector) remains invariant under head roll. Figure 1*B, I,* illustrates this case for a hypothetical neuron with a leftward preferred direction. For all head roll positions, the d-vector (white upward arrow) points upward with respect to the head.

II. If the preferred direction of eye displacement stays invariant relative to the eye orientation (and therefore to a target on the retina), the *frame of reference* for eye displacement is *oculocentric* and deviates from the head-fixed reference frame by the amount of OCR (see Fig. 1*B, II*). The illustrated preferred direction of the hypothetical neuron (upward white d-vector) is not invariant with respect to the head, but follows OCR (as indicated by the dotted coordinate frame).

We introduce a rotation coefficient c to quantify the amount of rotation of the preferred direction (in eye displacement) with respect to OCR. Then, $c = 0$ indicates the craniocentric (I), and $c = 1$ the oculocentric reference frame hypothesis (II).

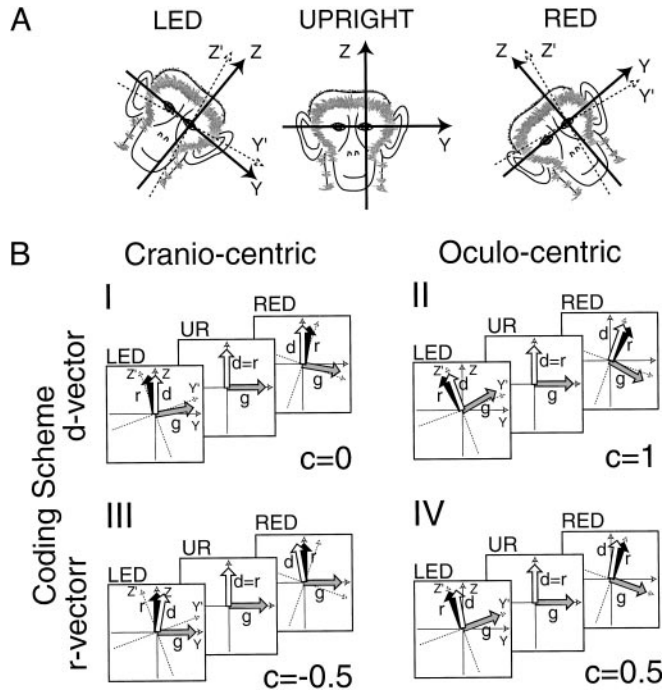

FIG. 1. Roll orientations of the eye and of hypothetical coordinate frames of paramedian pontine reticular formation (PPRF) saccade coding. *A*: craniocentric (bold axes: *Y, Z*) and oculocentric coordinate (dotted axes: *Y′, Z′*) frames overlap for the head *upright,* but dissociate during head roll in the left-ear-down (LED) and right-ear-down (RED) position due to ocular counterroll (OCR; exaggerated for clarity). *B*: hypotheses (I–IV) of a craniocentric and oculocentric representation of the eye displacement (d-vector, white arrow upward) and the eye rotation (r-vector, black arrow upward) coding scheme for a hypothetical PPRF burst neuron with a leftward preferred direction. Gaze shift (g-) vector shown in gray (positive *Y*-direction is leftward, see METHODS). *Hypothesis I*: eye displacement (d-vector) remains invariant during head roll with respect to craniocentric coordinates (*Y, Z*). Due to rotation kinematics, the corresponding eye rotation (r-) vector and the gaze (g-) vector, in contrast, rotate by ½ the amount of OCR. The rotation coefficient (change of d with respect OCR; see text) is zero: $c = 0$. *Hypothesis II*: d-vector remains invariant with respect to oculocentric coordinates (*Y′, Z′*), the rotation coefficient is $c = 1$. *Hypotheses III* and *IV*: craniocentric and oculocentric representation of the eye rotation (r-vector). Again, due to rotation kinematics, the eye displacement (d-) and eye rotation (r-) vector deviate by an angle of ½ the amount of OCR, leading to rotation coefficients of $c = -0.5$ and $c = 0.5$, respectively. The gaze vector *g* always follows the r-vector representation in this 2-dimensional (horizontal-vertical) scheme.

The actual eye rotation (r-) vector deviates from the eye displacement (d-) vector by half the amount of OCR because of the nonzero torsion of eye positions during OCR (half-angle rule) (Tweed and Vilis 1990). Consequently, a craniocentric coding scheme of eye displacement does not coincide with a craniocentric scheme of eye rotation or of gaze shift (Haustein 1989), and vice versa. For example, if the eye rotation (r-) vector is assumed to be head-fixed (Fig. 1*B, III*), the corresponding displacement (d-) vector rotates with OCR with a gain of −0.5. Therefore the rotation vector coding assumption leads to two different hypotheses.

III. If the coding of the rotation vector is in a *craniocentric reference frame,* the preferred direction of eye rotation (or of gaze shift) remains invariant under head roll. This is illustrated in Fig. 1*B, III,* where the r-vector (black arrow) indicates the leftward preferred direction of a hypothetical cell. The r-vector

remains upright with respect to the head for all roll positions. The d-vector (white arrow), in contrast, is not head-fixed.

IV. Finally, if the preferred direction of eye rotation (or of gaze shift) stays invariant relative to the eye orientation, the coding is in an *oculocentric frame of reference.* The r-vector (black arrow) of a hypothetical premotor burst neuron deviates from the head-fixed system by the amount of OCR (Fig. 1*B, IV*).

Since a gaze shift is always perpendicular to the horizontal-vertical component of the eye rotation vector, hypotheses III and IV are equivalent to the assumption of a cranicentric or oculocentric representation of gaze. And since the d-vector deviates from the r-vector by half OCR, the rotation coefficient c (defined for eye displacement) is -0.5 for the craniocentric (III) and $+0.5$ for the oculocentric (IV) rotation vector assumption (Fig. 1*B, III* and *IV*).

In general, rotation vectors (r-vectors) describing saccadic eye movements have a nonzero torsional component that depends on the horizontal-vertical eye position at saccade onset (following the half-angle rule). This torsional component of the rotation vector will be ignored for the purpose of this study, since we are only concerned with changes of the r-vector projection in the horizontal-vertical plane.

In four rhesus monkeys, we recorded extracellular single-unit activity and stimulated electrically in the PPRF, while the static head roll position of the animals was varied using a three-dimensional turntable. We found that all three considered PPRF burst neuron classes (SBN, BTN, and LBN) had a preferred direction of eye displacement that was closely craniocentric, but changed significantly with OCR with about one-fourth to one-half of the amount of OCR. To explain this deviation of the PPRF neurons from a simple craniocentric representation, we simulated the effect of OCR on the muscle pulling direction in a simplified three-dimensional geometric model of the oculomotor plant. Part of this study has been presented in abstract form (Scherberger et al. 1998a,b).

METHODS

Subjects

Four rhesus monkeys (*Macacca mulatta*: *Cr, De, Sa,* and *Ta*) were prepared for extracellular single-unit recording and microstimulation. Surgical procedures were applied as described elsewhere in more detail (Suzuki et al. 1999). In short, anesthesia was initiated with Ketamine and pentobarbital sodium. Animals were intubated and breathed a mixture of O_2 and N_2O, and supplemented with Halothane when required. Head bolts were chronically implanted for stable head fixation. A custom-made dual search coil was chronically implanted on one eye (Hess 1990). Finally, a recording chamber was placed on the surface of a trephine hole in the skull that was stereotaxically located on top of the PPRF region.

During the course of the experiment, the monkeys were head-restrained, such that in an upright position the horizontal stereotaxic plane of the head was pitched nose-down 15° with respect to the earth-horizontal plane. This placed the response plane of the horizontal semicircular canals orthogonal to the gravity vector (Böhmer et al. 1985).

Procedures and animal care were in accordance with the guidelines set by the Veterinary Office of the Canton of Zurich and the *Guide for the Care and Use of Laboratory Animals* (National Academy of Sciences 1996).

Setup

Awake monkeys were seated in a three-dimensional turntable that could be moved in various roll positions by computer control (Henn et al. 1992). The seat was arranged such that the center of the interaural line of the monkey's head was located at the intersection of the three chair rotation axes.

We recorded three-dimensional eye position with the dual search-coil technique, consisting of a large directional coil and a smaller, secondary coil for the measurement of eye torsion rigidly attached together and sealed (Hess 1990). A coil frame (31 cm diam) with two alternating magnetic fields in spatial and phase quadrature (Skalar Instruments, Delft, The Netherlands) was centered on the monkey's interpupillary line. The monkeys were trained to fixate targets (Wurtz 1969), which were used for the calibration of the eye position signal at the beginning of each experimental session (Hess et al. 1992).

For single-unit recording and electrical microstimulation in the PPRF, we used varnished tungsten microelectrodes, custom-made or commercial (FHC), with an impedance of 1.5–2 MΩ at 1 kHz. We recorded from saccade-related burst neurons, i.e., neurons presenting a short, transient burst prior to and during saccadic eye movements. Neurons were classified off-line as described below. To detect single-unit spikes, the amplified and band-filtered signals (0.5–10 kHz) were sent through a threshold discriminator, whose operation was constantly monitored on an oscilloscope. Detected spikes were electronically converted into an analog staircase signal, such that each spike was represented by a single step. This analog signal as well as the eye and the turntable position signals were then recorded at a sample rate of 833 Hz.

For electrical stimulation, 0.2-ms negative rectangular pulses at 500 Hz were repeated every 2 s in trains of 70 ms duration. Stimulation currents were well above threshold (20–100 μA) and typically in the order of 50 μA. At each site, stimulation intensity was kept constant for the entire testing in all roll positions.

Experimental protocol

Single-unit recording and electrical microstimulation in the PPRF was performed while monkeys made spontaneous eye movements in the light. The animals were motivated to perform saccades throughout the oculomotor range by presenting natural visual and auditory stimuli in the visual field, e.g., fruits, or movements of the experimenter. During each experiment, the animal was rotated from the upright to left-ear-down (LED) and right-ear-down (RED) static roll positions, typically up to 60° (40–90°) to either side.

Anatomical localization

The following oculomotor landmarks were electrophysiologically localized: SC was found below the fourth ventricle by identifying ocular motor burst units with activity for contralateral saccades and its typical topographic map. The trochlear nucleus was identified about 5 mm ventral to the SC where neurons showed eye-position–dependent tonic activity maximal for downward and intorsional eye positions. The abducens nucleus was localized about 10–12 mm ventral to the SC where neurons had burst-and-tonic activity with the preferred direction ipsilateral horizontal. The PPRF was localized rostral and dorsal to the abducens nucleus with a rostral extension of about 3 mm. SBN, BTN, and LBN were found intermingled in the PPRF.

After termination of the experiments, the monkeys were given an overdose of pentobarbital and perfused (paraformaldehyde 4%). One to 3 wk prior to perfusion, a chemical lesion (kainic acid) was set in the brain stem of three of the animals (*Cr, Sa,* and *Ta*) as part of a lesion experiment. Histological anatomy of the brain stem (Nissl and Golgi staining) identified lesion sites and recording tracks and was in agreement with the in vivo coordinates of the anatomical structures in all cases.

Data analysis

OCULAR COUNTERROLL. When the head is stationary in space, three-dimensional eye positions during fixation and saccades are confined to a Listing's plane (LP) that is defined by a constant amount of eye torsion. Static head roll shifts this plane along the torsional axis of the coordinate system normal to LP (Haslwanter et al. 1992). OCR was quantified by the amount of this torsional shift (Fig. 2). The angle between this eye torsional axis and the head roll axis was small ($<15°$), hence head roll stimulation was approximately orthogonal to LP.

SACCADE CHARACTERISTICS. On- and offsets of saccadic eye movements were automatically marked in the calibrated eye position signal on the basis of a velocity and acceleration criterion (software *Megadet*, Paul Hofman, Nijmegen, The Netherlands). All markings were visually confirmed and corrected if necessary (e.g., to eliminate blinks). For saccades evoked by microstimulation, care was taken to discard movements elicited closely before, during, or after spontaneous saccades.

For each saccade we defined the horizontal and vertical eye displacement (d-vector) as the difference between the eye position off- and onset, $d_H := H_{off} - H_{on}$ and $d_V := V_{off} - V_{on}$, where H_{on} (V_{on}) and H_{off} (V_{off}) denote the horizontal (vertical) axis components of the sacadic on- and offset positions as expressed in rotation vectors (Haustein 1989). As saccades stayed in Listing's plane, the torsional components were negligible. The direction Φ of a saccade was defined as $\Phi := \arctan(d_V/d_H)$. Thus $\Phi = +90°$ stands for a leftward, $\Phi = -90°$ for a rightward, and $\Phi = 0°$ for a downward saccade.

The three-dimensional eye rotation vector (r-vector) that describes the actual rotation of the eye from an initial eye position $r_{on} = (T_{on}, V_{on}, H_{on})^T$ to a target eye position $r_{off} = (T_{off}, V_{off}, H_{off})^T$ is given by $r = (r_{off} - r_{on} + r_{on} \times r_{off})/(1 + r_{on}^T \cdot r_{off})$, where T_{on} and T_{off} are the torsional components of the on- and offset eye position vectors r_{on} and r_{off} (Haustein 1989).

Since the saccadic path of large saccades was often not straight, we considered only small- and medium-sized saccades (amplitude $\leq 20°$) for our analysis to determine a cell's preferred direction most accurately.

NEURON ACTIVITY. Among the burst units in the PPRF, we distinguished short-lead burst neurons (SBN), burst-tonic neurons (BTN), and long-lead burst neurons (LBN) according to their firing pattern (Hepp and Henn 1983). All neurons showed a high-frequency burst activity prior to and during a saccade in the cell's preferred direction (mean firing rate for a 20° saccade typically about 400 Hz, always exceeding 200 Hz). In addition, BTN showed a tonic discharge rate during fixation periods that was eye-position dependent. We classified the three neuronal groups according to the time lead of the neuronal burst before saccade onset and the tonic firing rate during fixation. For this purpose, we examined the peri-saccadic spike density histogram (aligned to movement onset) of saccades not deviating more than 45° from the neuron's preferred direction (see PREFERRED DIRECTION below), and defined the beginning of the neuronal burst as the time when the cell's firing rate first exceeded one-third of its maximal burst activity, $t_{1/3}$. Following Hepp and Henn (1983), burst onset time was then compared with the saccade onset time, t_{on}. A unit was considered as a LBN if the beginning of the burst led the saccade onset by more than 12 ms ($t_{on} - t_{1/3} > 12$ ms). Otherwise the unit was considered to be either a SBN or BTN.

To quantify tonic firing rates, we analyzed, similar to Suzuki et al. (1999), eye fixation periods (typically 300) of 100 ms duration and starting 100 ms after the offset of spontaneous saccades. The mean tonic firing rate in these periods was correlated with the static eye position along the preferred direction, and a cell with $t_{on} - t_{1/3} \leq 12$ ms was classified as BTN, if the absolute linear regression slope significantly exceeded 1 Hz/deg ($P < 0.05$), otherwise it was classified a SBN. Following this criterion, we found no tonic discharge components in the LBN.

To determine the number of spikes associated with a saccadic burst, we counted, in the case of SBN and BTN, all spikes within a time interval extending from 10 ms prior to saccade onset up to 10 ms prior to saccade offset. For LBNs, a time window was selected that extended from 20 ms prior to saccade onset to 20 ms prior to saccade offset.

PREFERRED DIRECTION. For all selected saccades in a given static head roll position, we related the number of discharged spikes in a burst, n, to the horizontal and vertical saccade displacement component, d_H and d_V, with a piecewise linear model and, independently, also with a quadratic model (see RESULTS). In both cases the cell's preferred direction for each head roll position was determined from the parameters of the least-square optimized fit (Matlab procedure: leastsq). The overall fit quality was expressed by the coefficient of determination, $r^2 = 1 - [\Sigma (n - \hat{n})^2/\Sigma n^2]$, with n the measured and $\hat{n}$ the predicted number of spikes (Sachs 1984). The statistical reliability of this measure was tested using the bootstrap procedure (Efron and Tibshirani 1993), which generated a probability distribution and

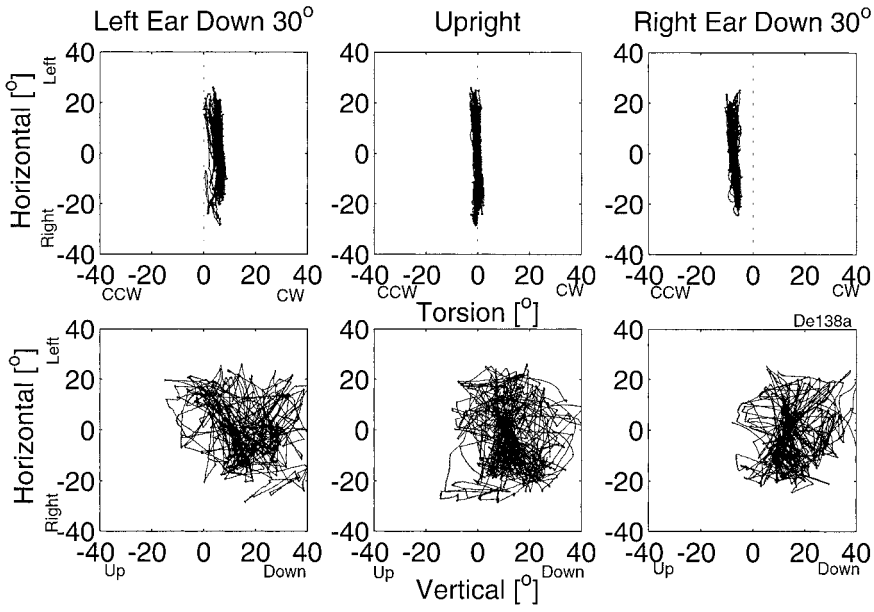

FIG. 2. Eye position trajectories in 3 dimensions. Recordings with the monkey rolled 30° left ear down (*left*), upright (*middle*), and 30° right ear down (*right*). *Top row*: the horizontal component of fixations and saccades vs. the torsional component. Note the torsional offset in the *left* and *right panels* in the clockwise (CW) and counterclockwise (CCW) direction indicating OCR. Dashed vertical lines mark 0° of torsion. The spread in the torsional component remains small in all 3 head orientations (standard deviation of data points from the best fit plane: 1.19°, 0.83°, 0.75°), demonstrating the conservation of Listing's law under head roll. *Bottom row*: the same horizontal components against the vertical eye position components. In all 3 head positions, the oculomotor range exceeds 50° in the horizontal and 40° in the vertical direction.

an estimate of the variance of r^2 by re-sampling the data 100 times. The preferred direction at a given head roll position was only further analyzed, if the underlying quadratic or piecewise linear fit was statistically reliable ($r^2 > 0.64$ with $P < 10^{-3}$).

ROTATION COEFFICIENT. For neurons with reliable fits in at least three different static head positions, a rotation coefficient c was calculated as the ratio of the change of the preferred direction Φ to OCR over all considered head positions (see RESULTS). The significance of this rotation coefficient was tested by bootstrap: re-sampling the data 100 times gave the probability distribution of the rotation coefficient c, which was considered significantly different from 0, if the mean of the distribution exceeded twice its standard deviation. The best-fit value of the whole sample was then taken as the final estimate of c. At the population level, the rotation coefficients in the three neural groups were checked against difference from 0 or 1 using t-tests.

RESULTS

Effect of static head roll

As expected, static head roll produced OCR, which we measured as the shift of Listing's plane along the torsional axis (Fig. 2). For any given head roll position, the eye torsion was approximately constant during saccades as well as during fixation periods. The standard deviation of the residual error of the linear fit was typically <1°. The ocular motor range was somewhat larger in the horizontal than the vertical component and exceeded 50 × 40°. This range was sufficiently large for a good estimate of LP and provided a variety of different saccade start- and endpoint locations.

Single-unit recordings

In four monkeys (*Cr*, *De*, *Sa*, and *Ta*), we recorded a total number of 82 saccade-related burst neurons while the static head roll was varied. In 59 of those neurons, the preferred direction could be determined with high significance ($r^2 > 0.64$ with $P < 10^{-3}$) in at least 3 head roll positions (LED, upright, and RED; range at least 60°) in both a piecewise linear (PL-) and a quadratic (Q-) model fit (see PIECEWISE LINEAR MODEL and QUADRATIC MODEL below). Only these neurons were further considered. According to our classification scheme, they split up in 31 SBN, 17 BTN, and 11 LBN (Table 1).

The preferred direction of these units was mainly ipsilateral horizontal (left- or rightward), but occasionally also vertical (3 units: up; 1 unit: down) or oblique (1 unit: 35° right-up). Head roll typically caused a change of the preferred direction in the direction of OCR. Figure 3 illustrates the change of the preferred direction, in head coordinates, in two PPRF neurons with the head 60° LED, upright, and 60° RED. Circles represent individual saccades with their position on the panel indicating the horizontal and vertical saccade displacement and their diameter proportional to the number of spikes of the burst. For a quantitative description of the preferred direction (arrows), we related the number of spikes during the saccadic burst, n, with the saccade displacement vector, (d_H, d_V), using both a piecewise linear and a quadratic model.

PIECEWISE LINEAR MODEL. In the piecewise linear (PL-) model, the number of spikes, n, was linearly related to the eye displacement vector, (d_H, d_V) and constrained by a lower limit, n_0, to prevent negative spike number predictions

$$n = \max\left[n_0, g_0 + g_1 \cos(\Phi_{PL}) \cdot d_H + g_1 \sin(\Phi_{PL}) \cdot d_V\right]$$

This model used four fit parameters (n_0, g_0, g_1, Φ_{PL}), determined by the least-square optimization procedure. n_0 predicts the (constant) number of spikes in the nonpreferred direction (baseline, close to 0). The parameters (g_0, g_1, Φ_{PL}) describe a linear function with intercept at the origin (g_0), the slope (g_1), and the direction of the steepest increase, or gradient, in the horizontal-vertical plane (Φ_{PL}). The preferred direction in the PL-model was then defined as Φ_{PL}. By this definition, $\Phi_{PL} = 90°$ indicated a leftward and $\Phi_{PL} = -90°$ a rightward saccade. The goodness-of-fit we quantified with the coefficient of determination, r^2, and for each neuron only those head roll positions were considered that provided a statistically reliable fit ($r^2 > 0.64$ with $P < 10^{-3}$; see METHODS).

Figure 4*A* shows a PL-fit of an SBN. Markers indicate spike counts over saccade displacement for individual saccades. The

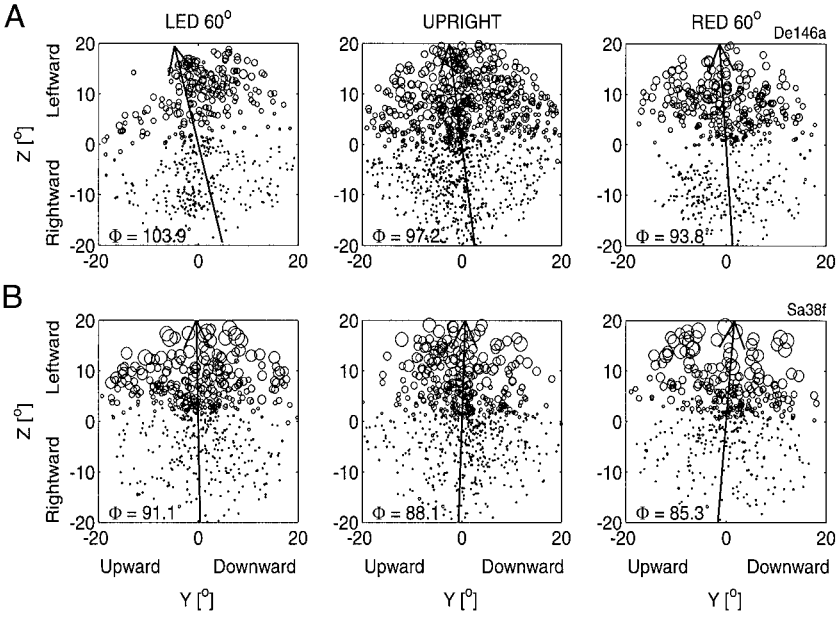

FIG. 3. Preferred direction of premotor burst neurons. Two neurons (*A*: *De146a; B*: *Sa38f*), each with the head 60° in the LED, upright, and 60° RED position. The location of each circle indicates the saccade displacement (d-vector) in the horizontal-vertical plane, whereas the size of each circle encodes the number of spikes in the saccadic burst. Small circles indicate none or a few spikes, the largest circles indicate 20 or more spikes. The preferred direction of the neuron (arrow), defined as the direction where spike numbers increase maximally, is not fixed, but rotates about 5° as the head rolls from the LED to the RED position (see Figs. 5 and 6 for a quantitative description).

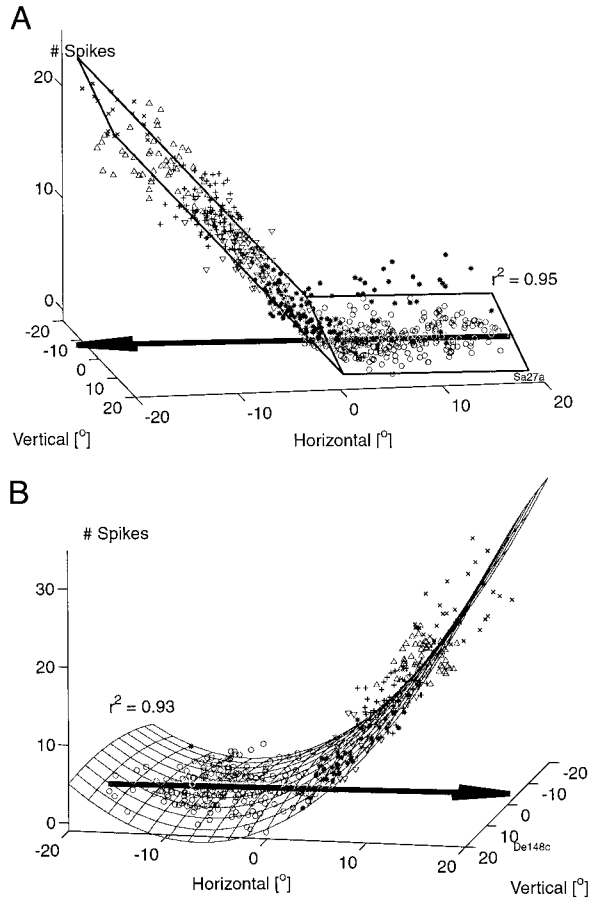

FIG. 4. Piecewise linear (*A*) and quadratic (*B*) model of single-unit burst activity. Three-dimensional plot shows the number of spikes during a saccadic burst of 1 single neuron as a function of the horizontal and vertical saccade component. Individual saccades are presented with different marker symbols according to the number of spikes per burst: ○, 0–1 spikes; *, 2–5; ▽, 6–9; +, 10–14; Δ, 15–19; ×, ≥20 spikes per burst. *A*: piecewise linear (PL-) model. Planes: surface of a 2-dimensional piecewise linear function least-square fitted to the data. The model consists of a linearly inclining plane and a horizontal plane acting as a lower limit. Arrow: preferred direction of the cell, defined as the upward direction of the inclining plane (*neuron Sa27a*). *B*: quadratic (Q-) model. Mesh: surface representation of a 2-dimensional quadratic function fitted to the data. Arrow: preferred direction of the cell, defined as the inclination direction of the quadratic surface at the origin (*neuron De148c*). The coefficient of determination (r^2) quantifies the overall goodness of the fit. Cells fire most vigorously for saccades in the preferred direction and are inactive for oppositely directed saccades (the increase of the Q-model in the anti-preferred direction is a model artifact).

inclining and the horizontal plane together represent the PL-fit to the data, while the arrow indicates the preferred direction.

As a measure of how much the cell's preferred direction of eye displacement was depending on head roll, we defined a rotation coefficient c_{PL} by the ratio of change of the preferred direction, Φ_{PL}, with OCR, given as the slope of the linear regression over all head roll positions: $c_{PL} := \Delta\Phi_{PL}/\Delta\text{OCR}$. By this definition, positive values of c_{PL} indicated a change of the preferred direction in the same direction as OCR, whereas negative coefficients indicated a change opposite to OCR, and $c_{PL} = 0$ a constant (head-fixed) preferred direction. To test for significance, we applied the bootstrap method (100 re-samples) and accepted c_{PL} as significantly different from 0, if the mean of the re-sampled distribution of c_{PL} exceeded twice its standard deviation (see METHODS).

Figure 5 illustrates the quality of the PL-fit for the same SBN as in Fig. 3*B*. The goodness-of-fit is shown in three (of 7 recorded) head roll position (*A–C*), as well as the dependence of the OCR and the cell's preferred direction, Φ_{PL}, from head roll (*D* and *E*). Finally, *F* demonstrates the linear relationship between the preferred direction and OCR. The rotation coefficient of this neuron (regression slope in *F*), c_{PL}, was 0.42 with a standard deviation of 0.09 (bootstrap re-sampling), and hence considered significantly different from zero (see METHODS).

Summarizing over all neurons, the rotation coefficient, c_{PL}, in the three cell groups had a mean of 0.24 ± 0.33 (mean ± SD) for the SBN, 0.29 ± 0.32 for the BTN, and 0.62 ± 0.73 for the LBN (see Table 1 and Fig. 7). The hypothesis of a head-centered reference frame of the eye displacement coding scheme (I, $c_{PL} = 0$) was rejected for all three groups (*t*-test, $P < 0.05$). The prediction of an eye-centered reference frame (II or IV, $c_{PL} = 1$ or $c_{PL} = 0.5$) was rejected for the SBN and BTN, indicating that the change of the preferred direction was significantly smaller than OCR ($c_{PL} < 1$), whereas the LBN group was not significantly different from the eye-centered assumption ($P = 0.11$).

Individually, 13 units (42%) of the SBN had a significantly positive rotation coefficient, while 17 SBN (55%) were not significantly different from zero, and 1 SBN (3%) had a rotation coefficient significantly negative. Four BTN (24%) and 5 LBN (45%) demonstrated a significant positive rotation, while the rotation coefficient in the remaining cells in both groups, 13 BTN (76%) and 6 LBN (55%), was not significantly different from zero. No BTN or LBN showed a significantly negative rotation coefficient (all *t*-tests, $\alpha = 0.05$).

Comparing the three cell populations, the rotation coefficient c_{PL} was neither significantly different between the SBN and the BTN (*t*-test, $P = 0.67$), nor between the BTN and the LBN group ($P = 0.10$). The difference between the LBN and the SBN group, however, was significant ($P = 0.03$).

QUADRATIC MODEL. Since these significant deviations of the preferred direction from a craniocentric reference frame were small, we analyzed the data also with a second, independent method. In the quadratic (Q-) model, we assumed a quadratic relationship between the component of the horizontal and vertical saccade displacement and the number of spikes of the sacadic burst

$$n = a_0 + a_1 d_H + a_2 d_V + a_3 d_H d_V + a_4 d_H^2 + a_5 d_V^2$$

where the parameters $a_0, \ldots, a_5$ were optimized by a least-square fit. Here the preferred direction of the cell, Φ_Q, was defined as the gradient direction of the fitted surface at the origin, i.e., $\Phi_Q = \arctan(a_2/a_1)$. Figure 4*B* shows the quadratic fit of an SBN with the preferred direction (arrow) as the steepest increase of the surface at the origin. A rotation coefficient was defined as $c_Q := \Delta\Phi_Q/\Delta\text{OCR}$, and the bootstrap method applied to test for significance (see METHODS). Figure 6, *A–C*, shows the goodness of the Q-fit for an LBN (same neurons as in Fig. 3*A*) in three (of 7 recorded) head roll positions as well as the dependence of OCR and of Φ_Q from head roll (*D* and *E*), and the dependence of the preferred direction from OCR (*F*). The rotation coefficient (regression slope in *F*) for this neuron was $c_Q = 0.66$.

Statistically, the results from the Q-model and PL-model were identical for the LBN, SBN, and the BTN group (Fig. 7).

TABLE 1. *Preferred direction and rotation coefficient of PPRF burst neurons*

	Q-Model				PL-Model			
Neuron	Phi	*c*	r^2	*n*	Phi	*c*	r^2	*n*
				SBN				
De121b	92.8	0.38 ± 0.06*	0.82	13	92.5	0.35 ± 0.08*	0.84	13
De122e	−92.5	0.38 ± 0.07*	0.84	6	−92.3	0.45 ± 0.07*	0.87	6
De129d	92.5	0.23 ± 0.12	0.82	8	91.8	0.26 ± 0.13	0.83	9
De144b	11.8	0.64 ± 0.13*	0.78	4	6.3	0.08 ± 0.17	0.82	3
De144d	87.9	0.40 ± 0.16*	0.84	3	86.9	0.41 ± 0.17*	0.85	3
De148c	91.2	0.23 ± 0.07*	0.90	7	90.7	0.29 ± 0.06*	0.92	7
De152c	96.0	0.24 ± 0.15	0.80	5	96.7	0.39 ± 0.17*	0.83	5
Cr53s7	−87.8	0.12 ± 0.26	0.83	3	−90.2	0.22 ± 0.28	0.86	3
Cr53s8	−87.9	0.49 ± 0.25	0.76	3	−89.8	0.47 ± 0.30	0.79	3
Sa11e	89.6	0.07 ± 0.15	0.77	7	89.4	0.12 ± 0.15	0.80	7
Sa12a	−96.9	0.80 ± 0.36*	0.84	3	−98.2	1.24 ± 0.46*	0.85	3
Sa12b	−102.0	0.22 ± 0.31	0.86	3	−101.6	0.07 ± 0.33	0.86	3
Sa13b	102.4	0.30 ± 0.26	0.79	3	100.8	0.32 ± 0.22	0.83	3
Sa23d	−88.4	0.01 ± 0.21	0.84	5	−89.2	0.08 ± 0.20	0.87	5
Sa24e	88.5	−0.11 ± 0.16	0.80	7	88.3	0.04 ± 0.17	0.83	7
Sa27a	−96.9	0.19 ± 0.11	0.90	7	−96.2	0.39 ± 0.13*	0.91	7
Sa28bc	−97.6	0.50 ± 0.19*	0.84	8	−98.4	0.53 ± 0.14*	0.87	8
Sa28e	−93.6	0.43 ± 0.10*	0.89	7	−93.3	0.30 ± 0.09*	0.93	7
Sa29a	−91.3	−0.14 ± 0.37	0.83	3	−91.1	−0.27 ± 0.36	0.83	3
Sa29b	−89.6	0.58 ± 0.18*	0.87	9	−90.0	0.46 ± 0.23*	0.88	9
Sa30a	103.1	−0.84 ± 0.26*	0.75	6	97.9	−0.73 ± 0.31*	0.74	7
Sa31a	94.8	−0.04 ± 0.25	0.83	4	94.3	−0.06 ± 0.28	0.86	4
Sa31b	93.6	0.65 ± 0.27*	0.75	8	93.7	0.52 ± 0.27	0.76	8
Sa35d	−90.2	−0.39 ± 0.31	0.71	5	−89.5	−0.13 ± 0.28	0.71	7
Sa35f	−97.3	0.23 ± 0.21	0.84	5	−97.0	0.20 ± 0.24	0.85	5
Sa36e	−100.2	0.20 ± 0.29	0.75	6	−97.1	0.25 ± 0.20	0.77	6
Sa37d	−97.9	0.60 ± 0.16*	0.88	7	−97.2	0.48 ± 0.16*	0.91	7
Sa38c	84.7	−0.46 ± 0.27	0.82	5	84.6	−0.11 ± 0.26	0.85	5
Sa38e	86.9	−0.07 ± 0.28	0.79	3	86.9	0.05 ± 0.27	0.82	3
Sa38f	88.1	0.37 ± 0.12*	0.89	7	87.8	0.42 ± 0.09*	0.92	7
Sa39a	88.3	0.44 ± 0.18*	0.83	7	88.0	0.46 ± 0.17*	0.88	7
		0.21 ± 0.35	**0.82**	**5.7**		**0.24 ± 0.33**	**0.84**	**5.8**
				BTN				
De117b	89.1	0.36 ± 0.22	0.75	6	88.9	0.40 ± 0.23	0.77	6
De138a	89.6	0.60 ± 0.07*	0.90	7	88.6	0.65 ± 0.08*	0.91	7
De149c	−99.6	0.45 ± 0.15*	0.79	7	−97.5	0.40 ± 0.17*	0.80	7
Cr23s3	88.1	0.33 ± 0.33	0.76	3	88.1	0.28 ± 0.32	0.77	3
Ta36s1	93.1	0.38 ± 0.20	0.83	3	92.0	0.33 ± 0.17	0.86	3
Ta36s6	92.2	0.46 ± 0.17*	0.80	3	91.5	0.47 ± 0.19*	0.81	3
Sa11d	−93.0	0.72 ± 0.39	0.86	3	−93.0	0.56 ± 0.31	0.89	3
Sa11f	−91.1	0.43 ± 0.21*	0.79	5	−90.8	0.22 ± 0.22	0.82	5
Sa13a	−88.7	0.47 ± 0.41	0.77	4	−88.7	0.61 ± 0.45	0.80	4
Sa15c	175.0	−0.22 ± 0.36	0.77	3	176.0	0.13 ± 0.53	0.73	3
Sa15d	91.7	0.30 ± 0.30	0.78	3	91.5	0.50 ± 0.33	0.81	3
Sa17b	94.6	0.53 ± 0.32	0.85	3	93.3	0.39 ± 0.29	0.88	3
Sa17c	91.7	−0.11 ± 0.13	0.86	7	91.2	0.01 ± 0.12	0.90	7
Sa17d	91.9	0.42 ± 0.23	0.79	3	91.5	0.51 ± 0.23*	0.83	3
Sa23b	−89.4	−0.02 ± 0.23	0.82	5	−87.9	0.24 ± 0.24	0.84	5
Sa24a	181.3	−0.32 ± 0.38	0.78	3	182.0	−0.46 ± 0.49	0.80	3
Sa36c	164.6	−1.14 ± 0.75	0.71	3	169.1	−0.39 ± 0.83	0.70	3
		0.21 ± 0.45	**0.80**	**4.2**		**0.29 ± 0.32**	**0.82**	**4.2**
				LBN				
De138b	−123.3	1.10 ± 0.15*	0.72	6	−125.4	1.00 ± 0.20*	0.72	6
De146a	97.2	0.66 ± 0.10*	0.83	7	97.8	0.75 ± 0.10*	0.87	7
De148d	86.5	0.15 ± 0.13	0.78	4	85.9	0.20 ± 0.16	0.77	5
Sa14c	89.1	0.02 ± 0.25	0.74	3	88.7	−0.02 ± 0.25	0.77	3
Sa24c	84.3	−0.34 ± 0.46	0.74	5	84.5	−0.09 ± 0.47	0.75	5
Sa28d	−91.9	0.44 ± 0.12*	0.80	7	−90.8	0.37 ± 0.14*	0.85	7
Sa35c	−88.6	1.90 ± 0.36*	0.70	5	−91.1	2.06 ± 0.50*	0.70	5
Sa38b	85.2	0.42 ± 0.45	0.84	3	84.2	0.45 ± 0.44	0.85	3
Sa38d	91.2	−0.10 ± 0.34	0.85	3	90.5	−0.09 ± 0.35	0.86	3
Sa46a	−80.5	1.85 ± 0.32*	0.73	6	−76.8	1.77 ± 0.50*	0.73	5
Sa62a	87.1	0.03 ± 0.19	0.79	6	85.5	0.43 ± 0.25	0.80	6
		0.56 ± 0.76	**0.78**	**5.0**		**0.62 ± 0.73**	**0.79**	**5.0**

Values in *c* are means ± SD. Three classes of neurons: short-lead burst neurons (SBN), burst-tonic neurons (BTN), and long-lead neurons (LBN). For both methods of analysis, Q- and PL-model, we show the neuron's preferred direction for the upright position, phi, the rotation coefficient, *c*, the coefficient of determination, r^2, and the number of head positions, *n*, in which the preferred direction was estimated reliably. Bold numbers: mean for each class. *, values significantly different from zero ($P < 0.05$).

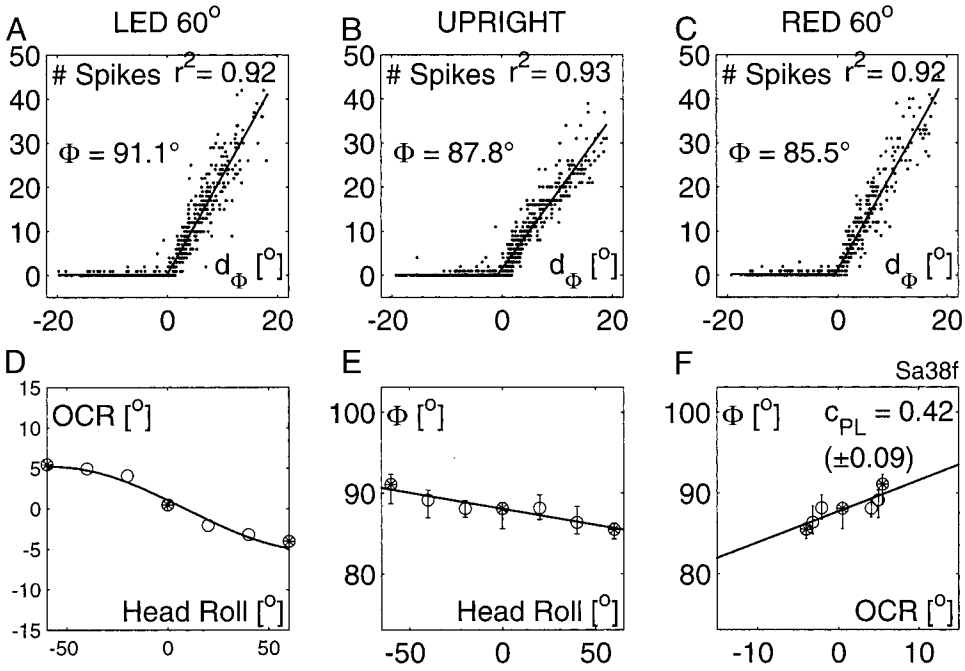

FIG. 5. Change of the preferred direction with OCR in the PL-model. *A–C*: neuronal burst activity and piecewise linear fit of a single neuron in various head roll positions: 60° LED, upright, and 60° RED (see Fig. 3*B* for the preferred direction of this neuron in these roll positions). In each panel, data and fit are shown from a perspective orthogonal to the preferred direction (Φ), hence d_Φ denotes the eye displacement component in the direction of Φ. Residual errors are small, as indicated by the coefficient of determination (r^2). *D*: ocular counterroll (OCR) as a sinusoidal function of head roll (recorded simultaneously with the neuron). *E*: variation of the preferred direction (Φ) with head roll. *F*: change of the preferred direction with OCR. The slope of the linear regression (straight line) defines the rotation coefficient *c* (±SD). Error bars: 95% confidence intervals of Φ. Exemplified data in *A–C* are highlighted in *D–F* (*neuron Sa38f*).

As the only difference, c_Q was not significantly different from zero in the BTN group, while c_{PL} was different. Comparing the goodness-of-fit in the Q- and the PL-model (Table 1), the coefficient of determination, r^2, was slightly lower in the Q-model than in the PL-model (mean r^2_Q/mean r^2_{PL}) 0.78/0.79 (LBN), 0.82/0.84 (SBN), and 0.80/0.82 (BTN), suggesting the PL-model to be at least as accurate as the Q-fit, even though the PL-model has only four free parameters, as compared with six in the Q-model. Individually, the rotation coefficients obtained by the two methods were also quite comparable with a correlation coefficient of 0.92 between c_Q and c_{PL} (Fig. 8*A*). Only 2 of 59 neurons had an absolute difference $|c_Q - c_{PL}|$ larger than 0.5. The PL- and the Q-model thus lead to the same results.

ROTATION (R-) VECTOR ANALYSIS. We also checked the PL-model with respect to the saccade rotation (r-) vector. Here, the number of spikes during a saccadic burst, *n*, was correlated to the horizontal and vertical component of the eye rotation vector, (r_H, r_V)

$$n = \max\left[n_0, g_0 + g_1 \cos\left(\Phi_{PL,r}\right) \cdot r_H + g_1 \sin\left(\Phi_{PL,r}\right) \cdot r_V\right]$$

and the preferred direction and the rotation coefficient, c_{PL}, determined as described above in the PL-model analysis. We found the rotation coefficients from the r-vector analysis exactly 0.5 larger than the rotation coefficients based on saccade displacement (Fig. 8*B*). Data points in the scatter plot $c_{PL,r}$ versus c_{PL} aligned tightly around the line "$y = x + 0.5$," as

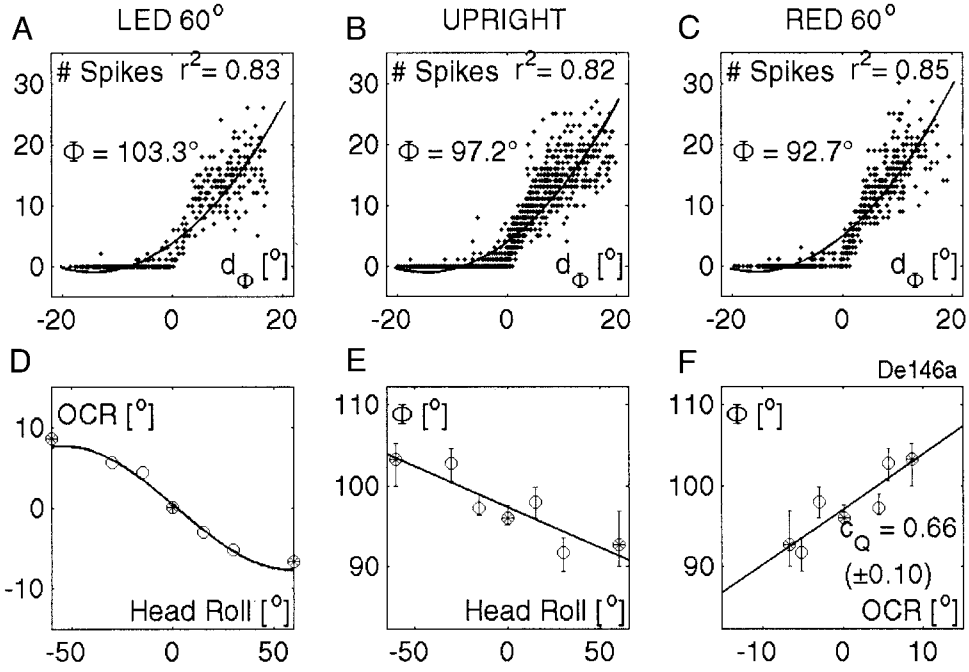

FIG. 6. Change of the preferred direction with OCR in the Q-model. *A–C*: neuronal burst activity and quadratic function fit of a single neuron in the 60° LED, upright, and 60° RED head roll position (see Fig. 3*A* for the preferred directions). Data and fitted model are shown from a perspective orthogonal to the preferred direction (Φ). d_Φ denotes the eye displacement component in the direction of Φ. r^2: coefficient of determination. *D*: OCR vs. head roll. *E*: variation of the preferred direction (Φ) with head roll. *F*: change of the preferred direction with OCR. The slope of the linear regression (straight line) defines the rotation coefficient *c* (±SD). Error bars show 95% confidence intervals. Exemplified data in *A–C* are highlighted in *D–F* (*neuron De146a*).

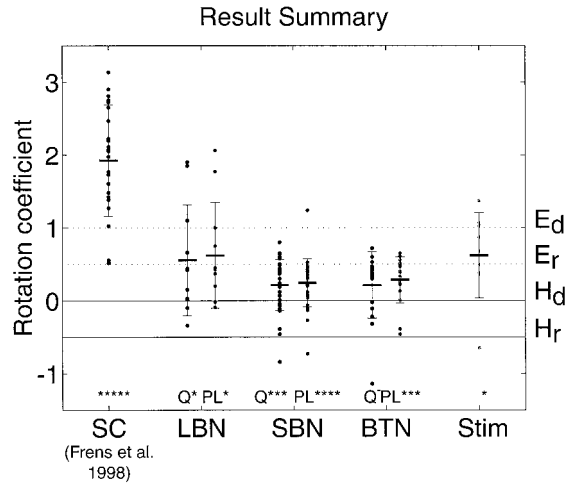

FIG. 7. Summary of the rotation coefficients obtained for the 3 neuronal subgroups [long-lead burst neurons (LBN), short-lead burst neurons (SBN), and burst-tonic neurons (BTN)] and for the electrical stimulation experiments (Stim). For comparison, the corresponding data for the superior colliculus (SC), as reported in Frens et al. (1998), is also shown. Vertical axis, rotation coefficient (with respect to eye displacement) in the Q-model (Q) and the PL-model (PL); dots, single neurons and simulation sites; horizontal bars, mean; error bars, SD; horizontal lines, rotation coefficients for craniocentric (solid) and oculocentric coordinates (dotted) both for the eye displacement (H_d, E_d) and the eye rotation coding scheme (H_q, E_q). Significance for nonzero rotation coefficient (*$P < 0.05$, **<0.01, *** <0.005, ****<0.001; —, not significant, $P > 0.05$).

expected from theoretical considerations of eye movement kinematics (see INTRODUCTION).

Microstimulation

In addition to single-unit recordings, we electrically stimulated the PPRF in two monkeys (*De* and *Sa*) at a total of 12 sites from which we had previously recorded. Immediately before stimulation, the presence of either single-unit signals or, as a minimum, saccade-related background activity was established. Electrical stimulation elicited ipsilateral horizontal eye movements in 9 of 12 sites (7 leftward, 2 rightward; see Table 2). The stimulation direction of the three other sites was oblique (40° right-up and twice 32° left-down from horizontal). Stimulation sites with oblique saccades were excluded from further analysis, since they most likely involved the stimulation

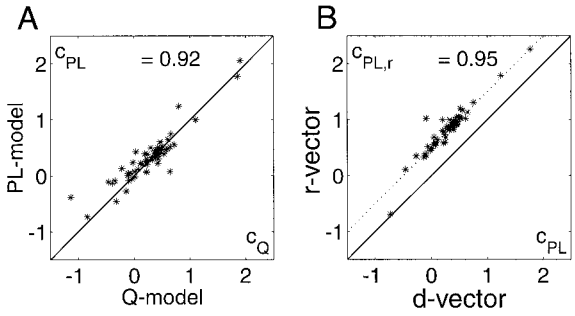

FIG. 8. *A*: correlation of rotation coefficients of the Q-model (c_Q) and the PL-model (c_{PL}), 59 neurons. Data points stay close to the unity line (correlation coefficient $\rho = 0.92$). *B*: correlation of rotation coefficients in the PL-model using the eye displacement signal (d-vector; c_{PL}) vs. the eye rotation signal (r-vector: $c_{PL,r}$). As predicted from eye rotation kinematics, coefficients derived from the r-vector are by 0.5 larger than those based on the d-vector (dotted line).

TABLE 2. *Average direction and rotation coefficient of evoked eye movements*

Neuron	Phi	Amplitude	*n*	*c*
De156b	89.1 ± 7.6	11.0 ± 3.3	9	1.06 (1.0, 1.2)
De157b	96.0 ± 5.1	11.2 ± 4.5	3	0.38 (0.2, 0.6)
De159a	78.9 ± 9.7	2.1 ± 0.9	9	0.49 (0.4, 0.6)
De161a	−81.5 ± 20.1	4.9 ± 2.4	9	−0.65 (−1.0, −0.3)
De161b	−84.4 ± 6.6	7.1 ± 2.2	9	0.87 (0.7, 1.1)
Sa41b	91.4 ± 8.5	7.6 ± 3.4	7	0.37 (0.0, 0.7)
Sa41c	96.8 ± 20.3	4.8 ± 2.0	7	0.68 (0.3, 1.1)
Sa42a	94.8 ± 26.0	8.9 ± 2.1	7	1.37 (0.6, 2.1)
Sa42b	89.5 ± 3.9	9.1 ± 1.4	7	1.02 (0.9, 1.1)

Values in Phi and Amplitude are means ± SD; numbers in parentheses are intervals. Rows indicate individual stimulation sites. Mean stimulation direction, phi, and mean stimulation amplitude, amp, for the head in the upright position. *n*, number of head roll positions for which the preferred direction was estimated. *c* (interval): rotation coefficient and its 95% confidence interval.

of additional oculomotor structures, e.g., bypassing axons, and not just PPRF burst neurons, whose preferred direction are predominantly horizontal.

To quantify the effects of stimulation, we determined the stimulation direction, Φ_{stim}, as the mean displacement direction of all elicited eye movements and defined, similar to the analysis of the neural recordings, a rotation coefficient c_{stim}: = $\Delta\Phi_{stim}/\Delta$OCR as the regression slope of the stimulation direction with OCR (Table 2, last column). The changes of the stimulation direction with head roll, c_{stim}, had a mean of 0.62 and a standard deviation of 0.58 over the 9 sites (Fig. 7). The mean was significantly different from the craniocentric (*t*-test, $P < 0.05$), but not from the oculocentric hypothesis in the eye displacement coding scheme ($P = 0.09$). Individually, 8 sites had a significantly positive and one site a significantly negative rotation coefficient.

The neural recording as well as the stimulation data provided evidence for co-variation of the preferred eye movement direction with OCR. This was true under the saccade displacement and even more so under the rotation coding assumption (Fig. 7). To better understand this deviation from a craniocentric representation in the premotor burst neurons, we simulated the effect of OCR on the pulling direction of horizontal extraocular eye muscles in a geometrical model of the oculomotor plant.

Oculomotor plant model

The pulling direction of extraocular eye muscles is restricted by connective tissue fibers (so-called pulleys) in the orbit (Demer et al. 1995, 2000; Miller and Robins 1987). The effect of muscle pulleys on the muscle pulling directions (or "muscle moments") depends on their orbital position and in particular on their relative location along the muscle path. OCR modifies the effective pulling direction since it changes the effective muscle path from the pulley to the muscle insertion on the globe. To demonstrate this effect, we simulated the pulling direction of individual horizontal eye muscles [medial rectus (MR) and lateral rectus (LR) muscle] in a simplified pulley model of the oculomotor plant with the eye straight-ahead. We studied both the assumption of *1*) orbit-fixed pulleys and *2*) of pulleys that rotate, to some extent, with OCR along the torsional axis.

Three-dimensional locations of the eye muscle origin and

insertion points were taken from anatomical measurements in the monkey (see Suzuki et al. 1999). Pulley positions were assumed along the muscle path with the eye straight-ahead and parameterized by relative muscle length (0: pulley position at the origin; 1: pulley at insertion). The effective pulling direction of the muscle and its projection on the horizontal-vertical plane, Φ_m, was then computed from the three-dimensional pulley and insertion position for any given OCR (see APPENDIX for further specifications).

ORBIT-FIXED PULLEYS. Under the assumption of an orbit-fixed pulley (*1*), the muscle moment changed with OCR, since OCR rotated the muscle insertion position in the orbit. The ratio $c_m := \Delta\Phi_m/\Delta\text{OCR}$ (m = MR, LR), which we call the rotation coefficient of the muscle, was therefore not zero in general. With no pulley (or with the pulley at the origin), the simulation showed a change of the muscle pulling direction close to the amount of OCR ($c_m \approx 1$; Fig. 9*A*). If the pulley was located further distal, i.e., closer to the muscle insertion, the rotation coefficient decreased: $c_m < 1$.

From the most recent and precise measurements (Demer et al. 2000), the pulleys of horizontal rectus muscles are posterior to the equator of the globe, and the distance of the pulleys to

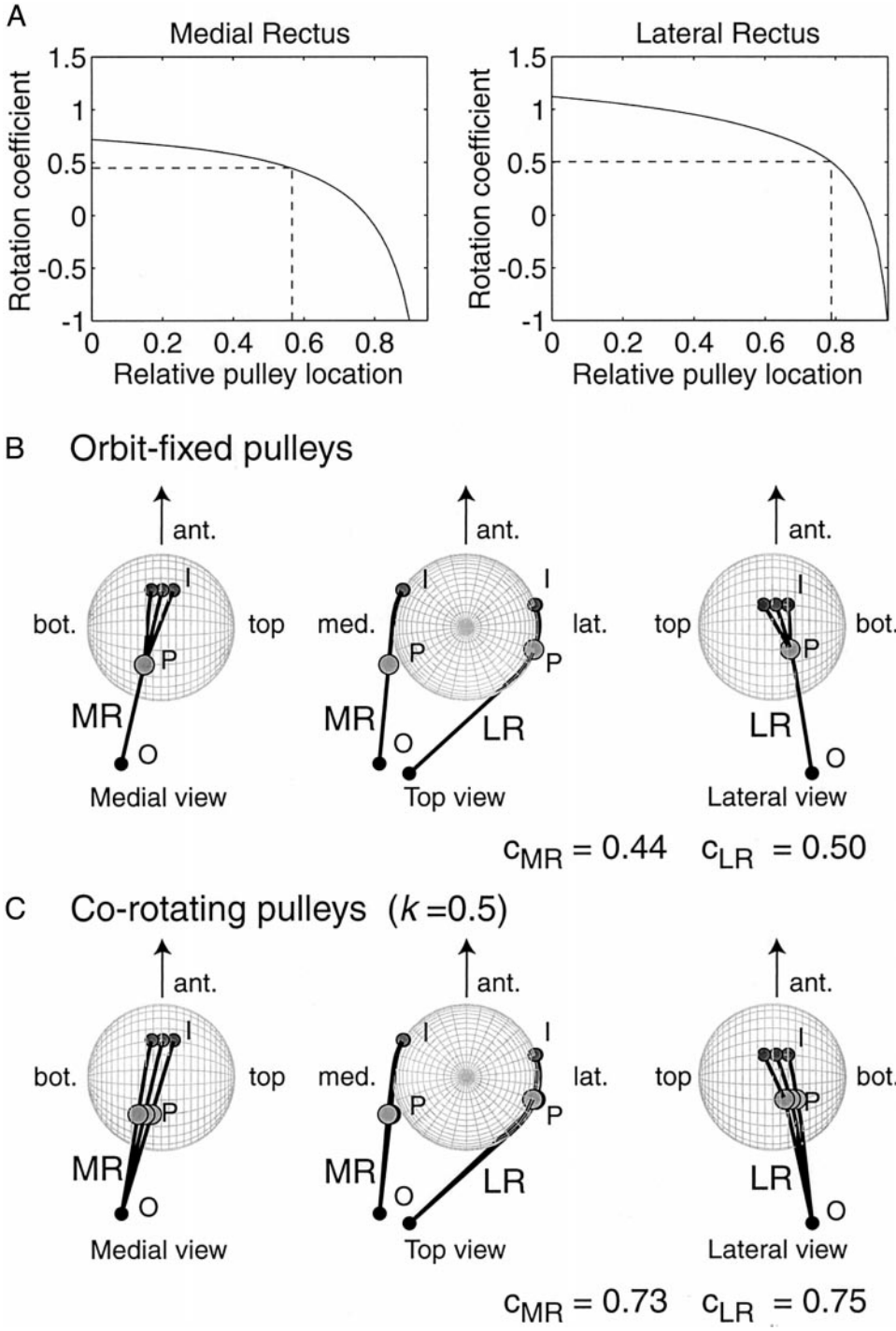

FIG. 9. Simulation of the change of muscle pulling direction with OCR for different pulley position and stiffness in horizontal extraocular eye muscles. *A* and *B*: pulleys fixed in the orbit. *C*: pulleys co-rotate with OCR. *A*: individual simulations for the medial rectus (MR) and lateral rectus (LR) muscle. Horizontal axis: relative pulley location (orbit-fixed) along the muscle path; 0, origin; 1, insertion. Vertical axis: rotation coefficient of the muscle pulling direction, defined as the relative change of pulling direction (in the horizontal/vertical plane) with OCR. Dotted lines: simulation for pulley locations after Demer et al. (2000), as shown in *B* and *C*. *B* and *C*: medial, top, and lateral view on a 3-dimensional geometric model of the right eye with the globe and both horizontal eye muscles (MR, LR). Anterior (ant.), medial (med.), lateral (lat.), bottom (bot.), and top margin of orbital space. O, muscle origin; P, pulley; I, muscle insertion for the eye upright and for ±10° OCR. Arrow: eye roll axis. *B*: pulley location fixed in the orbit. *C*: pulleys rotate with OCR along the torsional axis by ½ the amount of OCR (gain: k = 0.5).

the equator is about the same as the distance from the muscle insertion to the equator. This corresponds to a position at 57% (MR) and 79% (LR) of distal muscle extension in our model. [Such pulley positions correspond to *K*-values of 0.5 in Quaia and Optican (1998) and provide a mechanical implementation of Listing's Law.] Figure 9*B* illustrates the three-dimensional pulley location and the corresponding horizontal eye muscles paths for the upright eye position and for OCR of 10° to either side. The resulting muscle rotation coefficients were 0.44 for the MR and 0.50 for the LR muscle (Fig. 9*A*, dotted lines), which correspond to values of −0.06 (MR) and 0.0 (LR) in the rotation coefficient scheme of eye displacement of Fig. 7 [taking into account that the muscle pulling direction corresponds to the eye rotation (r-), not the eye displacement (d-) vector]. The observed coefficients in the PPRF output cells (SBN) are therefore significantly larger than the simulated rotation coefficients of the orbit-fixed pulley model. In fact, such a plant model would exactly predict a craniocentric representation of the d-vector scheme (I).

CO-ROTATING PULLEYS. The assumption of pulleys fixed in the orbit is not strictly valid. Demer et al. (2000) have demonstrated that extraocular eye muscle pulleys change their orbital position in the anterior-posterior direction as a function of the horizontal and vertical eye position, and hence are not completely fixed in the orbit. A torsional change in orbital pulley position during OCR has not been demonstrated, but cannot be excluded on the basis of orbital gross anatomy. The pulleys are embedded in a ring of connective tissue fibers, and the fascia of the vertical rectus muscles are in contact with the muscle fascia of the oblique eye muscles that control OCR. We therefore evaluated our plant model in addition under the assumption that the pulleys co-rotate with OCR.

A complete co-rotation with OCR (gain $k = 1$) would lead to a change of the muscle moment exactly following OCR and thus to a muscle rotation coefficient of 1 (or eye displacement coefficient of 0.5). A partial co-rotation of the pulleys with OCR seems more likely (due to elastic plant elements), and in lack of any experimental data, we simulated the plant for a co-rotation of half the amount of OCR (gain $k = 0.5$). Figure 9*C* illustrates the horizontal eye muscles path with nonorbit-fixed pulleys for the upright eye position and for OCR of 10° to either side. The simulated partial co-rotation with OCR resulted in a muscle rotation coefficient of 0.73 (MR) and 0.75 (LR), which corresponds to values of 0.23 (MR) and 0.25 (LR) in the eye displacement (d-vector) scheme of Fig. 7. Hence, a co-rotation of the pulleys with 50% of OCR would be compatible with the observed rotation coefficient of $c = 0.24$ in the SBN.

DISCUSSION

We asked the question in which reference frame presaccadic PPRF burst neurons use to encode rapid eye movements. For each of two coding scheme assumptions currently in discussion (the eye displacement vector scheme, where a saccade is encoded by the displacement of eye position, and the eye rotation vector scheme, where the actual eye rotation is encoded), we considered two possible anatomical frames of reference; a "craniocentric frame of reference," where the neuronal activity remains invariant under head roll (I and III), and an "oculocentric frame of reference," where the activity stays invariant to the eye orientation (II and IV; Fig. 1).

The torsional eye position, or OCR, remained constant for a given static head roll position (Fig. 2) as reported in previous studies (Haslwanter et al. 1992; Suzuki et al. 1997). Consequently, eye positions during spontaneous eye movements in the light were confined, in good approximation, to a two-dimensional horizontal-vertical plane, (the shifted) Listing's plane, for any static head position.

From single-unit recordings and electrical stimulation experiments, we found that single neurons as well as populations of PPRF neurons reorient their preferred direction with respect to the head (Fig. 3). The change in the output cells (SBN) was about 25% of the amount of OCR (Fig. 7). Hence, the data were close to the craniocentric reference frame in the eye displacement scheme (I); however, there was a consistent shift in the direction of OCR. Since this deviation from the craniocentric hypothesis was rather small, the question of measurement precision became particularly important. Therefore we measured the preferred direction for each neuron in many different roll positions (3–13; see Table 1) and analyzed the data in two independent ways, using a piecewise linear and a quadratic model (Figs. 4–7). For each model, a different definition of the neuron's preferred direction was chosen, but the resulting change of preferred direction with OCR was essentially the same (Figs. 7 and 8).

During electrical stimulation, the mean rotation coefficient through all sites roughly matched the mean value of the LBN (Fig. 7). The stimulation effect was not closely correlated with the rotation coefficients of the neurons recorded in the neighborhood of the stimulation site. A reason for the difference between the stimulation data and the single-unit results might be that electrical stimulation activates LBN, SBN, and BTN simultaneously due to their intermingled distribution in the PPRF. In addition, electrical stimulation could easily activate other eye-movement–related structures, like bypassing axons, and hereby lead to effects difficult to interpret. This is more likely in the PPRF than in the SC. The particular high standard deviation of the stimulation direction at some stimulation sites (see Table 2) might be due to such co-stimulation (excluding these sites did not alter our results). Bearing these differences in mind, it is still noteworthy that the electrical stimulation results were, like the single-unit data and unlike the SC results, in-between the craniocentric and oculocentric representation for eye displacement (Fig. 7).

We focused our analysis on the dependence of the preferred direction of PPRF neurons on eye torsion. The question, whether the preferred direction of PPRF neurons depends on the horizontal and vertical eye position is also of interest, as suggested by a recent model of visuo-motor transformation (Crawford and Guitton 1997). We were unable to detect a significant dependence of the (2-D) preferred direction from the horizontal or vertical eye position, neither for the eye displacement (d-) nor the eye rotation code (r-vector). However, such subtle changes as predicted by these models are difficult to detect for small- and medium-sized saccades.

The goodness-of-fit for the d- and the r-vector analysis was very similar, as expected for this two-dimensional analysis, and the rotation coefficient of the PPRF output cells (SBN) was right in between the craniocentric eye displacement (I) and the oculocentric eye rotation (IV) hypothesis ($c = 0.25$, Fig. 7). All

of the above did not provide additional evidence in favor of either the eye displacement or the eye rotation coding scheme assumption. However, the question of the appropriate coding scheme of saccades in premotor burst neurons is of central importance for a more complete understanding of the brain stem saccade generator and the visuo-motor signal transformation process in general (Crawford and Guitton 1997; Quaia et al. 1999; Tweed 1997) and will be addressed in an upcoming three-dimensional study of premotor saccadic burst neurons (Hepp et al. 1999).

Klier and Crawford (1998) studied the question whether eye torsion (OCR) leads to inaccurate saccades. They showed that the human oculomotor system compensates eye position effects under visual feedback, but saccade traces toward visual targets during OCR were initially misdirected and changed course toward the target only later during the movement. In our data set of spontaneous eye movements in the light (with saccade amplitudes not exceeding 20°), targets were not presented explicitly, and hence the question of target accuracy could not be addressed directly. However, saccade trajectories were essentially straight, and we did not observe an increased number of corrective saccades in the presence of OCR, which both could indicate a decrease in saccade accuracy. On the other hand, their finding that the torsional position compensation was not complete for saccades from OCR positions does correspond rather well with our finding that the burst neuron signals are not quite in head-fixed coordinates. One possible explanation for both effects might be that the oculomotor system is not optimally calibrated for saccades made in torsional eye positions.

Possible mechanisms

Presaccadic burst regions (PPRF and riMLF) receive input directly and indirectly from cortical areas (frontal eye field, lateral intraparietal cortex) as well as from subcortical structures including SC (for a review see Hepp et al. 1989). In the SC, the eye displacement command is encoded in an intermediate coordinate frame that is neither cranio- nor oculocentric, but has a strong bias to gravity (Fig. 7) (Frens et al. 1998). The nature of this coding scheme is not resolved. One possible explanation is that the cortical visual input to the SC is also biased toward gravity, as recently suggested (Sauvan 1998; Sauvan and Peterhans 1995). Such an interpretation would predict a corresponding shift in the tuning curves of cortical oculomotor areas, like the lateral intraparietal area (LIP) and the frontal eye fields (FEFs). In any case, the signal in the SC seems to represent neither pure retinal nor oculomotor error, which might reflect its imminent role in gaze control under head-free conditions (Sparks 1999).

The saccadic signal transforms from the SC to the PPRF to an almost craniocentric representation. For this transformation, a gravity or torsional-eye-position input signal is required at the level of the PPRF or upstream to it. It could originate, among other sources, directly from the otoliths, indirectly from the cerebellum, or from the brain stem neural integrator, which itself receives otolith input. Evidence for the presence of a more direct otolith signal is the finding that the preferred direction of PPRF burst neurons have considerable torsional components during *dynamic* roll stimulation, e.g., during sinusoidal body oscillations about a head sagittal (naso-occipital) axis (Hepp et al. 1999). Both the neural integrator of the brain stem and the cerebellum, however, contain information on the current amount of eye torsion, which is sufficient for the required coordinate transformation (Crawford and Vilis 1999; Quaia et al. 1999).

The finding that the LBN rotate stronger with OCR than the SBN (even though the difference is not statistically significant in our sample) goes in line with the view that LBN play an intermediate role between the SC and the SBN (Keller et al. 2000). Apart from the SBN, which project monosynaptically to the motoneurons (Büttner-Ennever and Henn 1976), we recorded from phasic BTN in the medial (or periMLF) PPRF, which are putative floccular projection neurons and do not directly connect to the motoneurons (Horn et al. 1999). For this reason, we analyzed SBN and BTN separately, but found their frame of reference to be the same.

We also investigated the preferred direction of burst neurons in the riMLF (see Hepp et al. 1999). Even though the preferred direction of the riMLF burst neurons seemed to rotate with OCR in the horizontal-vertical plane, this rotation was difficult to interpret because of the large torsional components of the riMLF burst neurons. Therefore, in this study, we focused on saccade-related burst neurons in the PPRF, which contained less torsional activity.

Influence of the oculomotor plant

The significant deviation of the SBN from a craniocentric reference frame could reflect properties of the oculomotor plant. To test this hypothesis, we simulated the change of the muscle pulling direction (in the horizontal-vertical plane) during OCR (Fig. 9). The model revealed that the rotation coefficient of the SBN group could be matched with the rotation coefficients of the horizontal eye muscles for eye muscle pulley locations, consistent with anatomical measurements (Demer et al. 2000) and theoretical studies (Quaia and Optican 1998; Raphan 1998), if the additional assumption was made that the pulleys are not fixed in the orbit but rotate with OCR to some degree (50% in our simulation). It is therefore possible that the small deviation from a craniocentric reference frame in the neural representation of the output layer of the PPRF (SBN) corresponds to the change of the pulling direction of the horizontal eye muscles with OCR.

Precise pulley locations and the amount of pulley stiffness are not well established, in neither monkey nor man. For this reason, we kept our model as simple as possible and restricted it to the straight-ahead eye position. The assumption that the pulleys rotate with OCR in the orbit is, to our knowledge, not yet experimentally supported. Such an effect is certainly possible on the basis of the anatomy of the connective tissue ring in the orbit and its close relationship to the oblique eye muscles. Also, it has recently been shown (Demer et al. 2000) that rectus muscle pulleys change their orbital (anterior-posterior) position when the eye is moved in the horizontal or vertical direction.

The pulley effects of the vertical muscles (superior and inferior rectus) are also important for oculomotor plant kinematics. Simulations for the vertical rectus muscles with our model revealed very similar results as for the MR. However, as we present no corresponding neural data here, they are not shown.

Since rectus muscle motoneurons actually drive the eye muscles, their preferred directions are expected to closely reflect the effective muscle moments (Suzuki et al. 1999). It is unclear, however, whether motoneurons also show a change of preferred direction under OCR similar to the burst neurons in the PPRF. Studying the preferred direction of extraocular motoneurons under OCR would be of considerable interest, although it seems technically quite challenging to record from motoneurons in different static roll positions for a prolonged period of time. So far, it remains open whether output neurons of the PPRF share the same reference frame as the motoneurons and the oculomotor plant, or whether an additional coordinate transformation is present at the level of the motoneurons.

We conclude that saccadic eye movement commands, which are encoded in a representation in the SC in between an oculocentric and head-fixed representation, are transformed to a representation in the PPRF that is closely craniocentric. The small but significant modulation of the preferred direction with OCR could reflect, either fully or in part, the modulation of the horizontal eye muscle pulling direction with OCR.

APPENDIX

Specification of the geometric plant model

Suzuki et al. (1999, their Tables 1 and 2) reported three-dimensional positions of the origins and insertions of all six extraocular eye muscles of four monkey eyes, together with an average of these measurements in an idealized right eye. Following their method of anatomical description, we centered a stereotaxic coordinate frame (*x, y, z*) in the middle of the globe of an idealized right eye. Hereby, the *x*-axis was pointing forward and the *y*-axis horizontally leftward in Reid's plane, while the *z*-axis was normal to Reid's plane and pointing upward. The previously reported coordinates were assigned to the matrix variables *origin* and *insertion* in the following Matlab code (see function *get_phi* below).

We assumed in our model that the eye globe is spherical and that the eye muscles follow geodesic paths from the origin to a muscle pulley, from there to a tangential point on the globe (if the pulley is not on the globe), and from there along the surface of the globe to its insertion point. A pulley was assumed to control the path of each horizontal eye muscle, and its position set on the geodesic muscle path with the eye straight ahead. The pulley position was quantified as the relative path length along the muscle starting from the origin by a parameter $\lambda \in [0, 1]$. Hence, $\lambda = 0$ located the pulley at the origin, $\lambda = 0.5$ along the muscle path halfway between origin and insertion, and $\lambda = 1$ at the insertion point. In our first set of simulations (*1*), the pulleys were presumed to be fixed in the orbit. In contrast, in the second set (*2*) the pulleys were presumed to co-rotate with OCR along the *x*-axis with a fixed gain k ($0 \leq k \leq 1$).

The effective muscle pulling direction for any given eye position followed a geodesic path from the pulley (stable in the orbit for any given amount of OCR) to the insertion point (fixed on the globe). The direction of the three-dimensional muscle moment was described as the unit-vector (u_x, u_y, u_z) that is normal to the plane spanned by the muscle pulley, the muscle insertion, and the center of the globe (and its vector orientation following the right hand rule). Finally, the pulling direction in the horizontal-vertical plane was expressed as the angle $\Phi_m = \arctan(u_z/u_y)$ for m = MR, LR.

The Matlab function *get_phi* computes Φ_m for the eye looking straight ahead and in various amounts of OCR. For each of the horizontal eye muscles m (and a fixed pulley position λ and gain k), we defined a rotation coefficient $c_m := \Delta\Phi_m/\Delta\text{OCR}$ as the regression of Φ_m against OCR (varying $\pm 10°$). This was implemented in the function *rot_coef* (see below). For the pulleys fixed in the orbit (*1*), the gain was set to $k = 0$, while we demonstrated the case of co-rotating pulleys (*2*) with a gain of $k = 0.5$.

Matlab code

```
function phi = get phi(ocr, lambda, k, muscle)
% computes muscle moment direction in the yz-plane
% (phi = 0 deg; downward, phi = 90 deg: leftward)
% Input: ocr: ocular counterroll (in deg)
% lambda: relative pulley location (range 0-1)
% k: gain of pulley co-rotation with OCR (range 0-1)
% muscle number: "1" for MR, "2" for LR, "3" for SR, "4" for IR
origin = [% muscle origins: columns: MR LR SR IR IO SO, rows:
          % x, y, z coordinates
-17.80   -19.08   -18.30   -18.15    4.80    7.08
 11.28     7.40     9.15     9.23    2.08    6.70
 -5.13    -5.15    -1.60    -7.08   -11.80   8.78];
                                  % (see Suzuki et al. 1999)
insertion = [% muscle insertions: columns: MR LR SR IR IO SO,
              % rows: x, y, z coordinates
4.86     2.91     3.71     4.22    -8.27    -5.53
8.25    -9.11    -2.14    -0.91    -4.74    -2.19
0.22    -0.44     8.57    -8.55    -0.95     7.51];
                                  % (see Suzuki et al. 1999)
org = origin(:, muscle);   % origin of selected muscle
norg = norm(org);   % distance of origin from center of the globe
I_zero = insertion(:, muscle);   % insertion of selected muscle in
                                 % primary position
r = norm(I_zero);   % radius of the globe
a = ocr* pi/180;   % angle of OCR in radiant
M = [1 0     0   % matrix representing roll axis rotation of OCR
   0 cos(a) -sin(a)
   0 sin(a) cos(a)];
I = M*I_zero;   % muscle insertion point at OCR position
% calculate muscle tangential point in primary position
n_zero = org * (r*r)/(norg^2);
m_zero = cross (I_zero, org);
r_zero = r*sqrt(1 - r*r/(norg^2));
s_zero = cross(org, m_zero); s_zero = s_zero/norm(s_zero);
T_zero = n_zero + r_zero * s_zero;   % muscle tangential point
                                     % in primary position
% calculate muscle pulley location according to its distal fraction
% lambda along the muscle path in primary position
1_g = norm(T_zero - org);   % distance of origin from tangential
                            % point
arc = acos(dot(T_zero, I_zero)/(norm(T_zero)*norm(I_zero)));
1_a = r*arc;   % path distance between tangential point and
               % muscle insertion along the globe
len = 1_g + 1_a;   % total muscle length
lambda_t = 1_g/len;   % linear fraction of the muscle path
if lambda <= lambda_t;   % pulley is on the linear part of the
                         % muscle
  mu = lambda/lambda_t;   % re-normalize to linear fraction
  P = mu*T_zero + 1-mu)*org;   % 3-D pulley location
else      % pulley is on the global part of the muscle
  mu = (lambda - lambda_t)/(1-lambda_t);
       % re-normalize to global muscle fraction
  rl = cross(T_zero, I_zero);   % vector normal to muscle plane
  T_ort = cross(rl, T_zero); T_ort = r*T_ort/norm(T_ort);
          % vector in the muscle plane
          % and normal to the tangential point
  P = cos(mu*arc) *T_zero + sin(mu*arc) *T_ort;
       % 3-D pulley location
end
P = [ 1 0    0   % rotating pulley with angle a*k
```

```
    0 cos(a*k) -sin(a*k)
    0 sin(a*k) cos(a*k)]*P;
n_p = P*(r*r)/(norm(P)^2);  % get direction of muscle moment
m = cross(I,P); m = m/norm(m);  % muscle moment
phi = cart2pol(m(3), -m(2))*180/pi;
        % muscle moment direction (in degree) in the yz-plane
phi_zero = cart2pol(m_zero(3), -m_zero(2))*180/pi;
        % avoid 360 deg periodicity jump here
if ((abs(phi_zero) > 150) & (phi < 0)) phi = phi + 360; end;
return;
function c = rot_coef(lambda, k, muscle)
        % get rotation coefficient: delta_PHI/delta_OCR
ocr = [-10:0.5:10]';  % assume a set of OCR positions
for i = l:length(ocr)  % compute muscle moment directions (PHI)
                       % for each OCR position
  phi(i) = get_phi(ocr(i), lambda, k, muscle);
end;
params = regress(phi', [ocr ones(size(ocr))];  % linear regression
c = params(l);  % rotation coefficient is the regression slope of
                % PHI vs. OCR
return;
```

We thank B. Hess for helpful discussions and administrative support, P. Hofman for providing the saccade-detection program *Megadet*, and B. Disler, S. Elsässer, V. Furrer-Isoviita, and R. Stocker for excellent technical assistance. We also thank J. Büttner-Ennever and A. Horn for histological verification of the recording and stimulation sites, and two anonymous referees for excellent comments that greatly improved the manuscript.

This work was supported by the Swiss National Foundation, Esprit II (31-40484.94).

REFERENCES

BÖHMER A, HENN V, AND SUZUKI JI. Vestibulo-ocular reflexes after selective plugging of the semicircular canals in the monkey-response plane determination. *Brain Res* 326: 291–298, 1985.

BÜTTNER U, BÜTTNER-ENNEVER JA, AND HENN V. Vertical eye movement related activity in the rostral mesencephalic reticular formation of the alert monkey. *Brain Res* 130: 239–252, 1977.

BÜTTNER-ENNEVER JA AND BÜTTNER U. A cell group associated with vertical eye movements in the rostral mesencephalic reticular formation of the monkey. *Brain Res* 151: 31–47, 1978.

BÜTTNER-ENNEVER JA AND HENN V. An autoradiographic study of the pathways from the pontine reticular formation involved in horizontal eye movements. *Brain Res* 108: 155–164, 1976.

COHEN B, KOMATSUZAKI A, AND BENDER MB. Electrooculographic syndrome in monkeys after pontine reticular formation lesions. *Arch Neurol* 18: 78–92, 1968.

CRAWFORD JD. The oculomotor neural integrator uses a behavior-related coordinate system. *J Neurosci* 14: 6911–6923, 1994.

CRAWFORD JD AND GUITTON D. Visual-motor transformations required for accurate and kinematically correct saccades. *J Neurophysiol* 78: 1447–1467, 1997.

CRAWFORD JD AND VILIS T. Role of the primate 3-D neural integrator in ocular counteroll during head tilt. *Soc Neurosci Abstr* 25: 8.7, 1999.

DEMER JL, MILLER JM, POUKENS V, VINTERS HV, AND GLASGOW BJ. Evidence for fibromuscular pulleys of the recti extraocular muscles. *Invest Ophthalmol Vis Sci* 36: 1125–1136, 1995.

DEMER JL, OH SY, AND POUKENS V. Evidence for active control of rectus extraocular muscle pulleys. *Invest Ophthalmol Vis Sci* 41: 1280–1290, 2000.

EFRON B AND TIBSHIRANI RJ. *An Introduction to the Bootstrap.* New York: Chapman and Hall, 1993.

FERMAN L, COLLEWIJN H, AND VAN DEN BERG AV. A direct test of Listing's law. II. Human ocular torsion measured under dynamic conditions. *Vision Res* 27: 939–951, 1987.

FRENS MA, SUZUKI Y, SCHERBERGER H, HEPP K, AND HENN V. The collicular code of saccade direction depends on the roll orientation of the head relative to gravity. *Exp Brain Res* 120: 283–290, 1998.

FUCHS AF AND LUSCHEI ES. Firing patterns of abducens neurons of alert monkeys in relationship to horizontal eye movement. *J Neurophysiol* 33: 382–392, 1970.

HASLWANTER T, STRAUMANN D, HEPP K, HESS BJ, AND HENN V. Smooth pursuit eye movements obey Listing's law in the monkey. *Exp Brain Res* 87: 470–472, 1991.

HASLWANTER T, STRAUMANN D, HESS BJM, AND HENN V. Static roll and pitch in the monkey: shift and rotation of Listing's law. *Vision Res* 32: 1341–1348, 1992.

HAUSTEIN W. Considerations on Listing's law and the primary position by means of a matrix description of eye position control. *Biol Cybern* 60: 411–420, 1989.

HELMHOLTZ H. *Handbuch der Physiologischen Optik.* [Translated in English (1924, 1962) *Treatise on Physiological Optics.* New York: Dover.] Leipzig, Leopold Voss, 1867.

HENN V AND COHEN B. Coding of information about rapid eye movements in the pontine reticular formation of alert monkeys. *Brain Res* 108: 307–325, 1976.

HENN V, STRAUMANN D, HESS BJM, HASLWANTER T, AND KAWACHI N. Three-dimensional transformation from vestibular and visual input to oculomotor output. *Ann NY Acad Sci* 656: 166–179, 1992.

HEPP K, CABUNGCAL JH, DUERSTELER M, HESS BJM, SCHERBERGER H, STRAUMANN D, SUZUKI Y, VAN OPSTAL J, AND HENN V. 3D structure of the reticular saccade generator. *Soc Neurosci Abstr* 25: 661.6, 1999.

HEPP K AND HENN V. Spatio-temporal recording of rapid eye movement signals in the monkey paramedian pontine reticular formation (PPRF). *Exp Brain Res* 52: 105–120, 1983.

HEPP K, HENN V, VILIS T, AND COHEN B. Brainstem regions related to saccade generation. In: *The Neurobiology of Saccadic Eye Movements,* edited by Wurtz RH and Goldberg ME. New York: Elsevier, 1989.

HEPP K, VAN OPSTAL AJ, SUZUKI Y, STRAUMANN D, HESS BJM, AND HENN V. Listing's Law. Visual, motor or visuomotor? In: *Three-Dimensional Kinematics of Eye, Head and Limb Movements,* edited by Fetter M, Haslwanter T, and Misslisch H. Amsterdam: Harwood Academic, 1997.

HESS BJM. Dual-search coil for measuring 3-dimensional eye movements in experimental animals. *Vision Res* 30: 597–602, 1990.

HESS BJM, VAN OPSTAL AJ, STRAUMANN D, AND HEPP K. Calibration of three-dimensional eye position using search coil signals in the rhesus monkey. *Vision Res* 32: 1647–1654, 1992.

HORN AK, BÜTTNER U, AND BÜTTNER-ENNEVER JA. Brainstem and cerebellar structures for eye movement generation. *Adv Otorhinolaryngol* 55: 1–25, 1999.

KELLER EL. Participation of medial pontine reticular formation in eye movement generation in monkey. *J Neurophysiol* 37: 316–332, 1974.

KELLER EL, MCPEEK RM, AND SALZ T. Evidence against direct connections to PPRF EBNs from SC in the monkey. *J Neurophysiol* 84: 1303–1313, 2000.

KING WM AND FUCHS AF. Reticular control of vertical saccadic eye movements by mesencephalic burst neurons. *J Neurophysiol* 42: 861–876, 1979.

KLIER EM AND CRAWFORD JD. Human oculomotor system accounts for 3-D eye orientation in the visual_ motor transformation for saccades. *J Neurophysiol* 80: 2274–2294, 1998.

LUSCHEI ES AND FUCHS AF. Activity of brain stem neurons during eye movements of alert monkeys. *J Neurophysiol* 35: 445–461, 1972.

MAYS LE AND SPARKS DL. Saccades are spatially, not retinocentrically, coded. *Science* 208: 1163–1165, 1980.

MILLER JM AND ROBINS D. Extraocular muscle sideslip and orbital geometry in monkeys. *Vision Res* 27: 381–392, 1987.

NATIONAL ACADEMY OF SCIENCES. *Guide for the Care and Use of Laboratory Animals* (7th ed.), National Research Council, Institute for Laboratory Animal Research, NAS, 1996.

QUAIA C, LEFEVRE P, AND OPTICAN LM. Model of the control of saccades by superior colliculus and cerebellum. *J Neurophysiol* 82: 999–1018, 1999.

QUAIA C AND OPTICAN LM. Commutative saccadic generator is sufficient to control a 3-d ocular plant with pulleys. *J Neurophysiol* 79: 3197–3215, 1998.

RAPHAN T. Modeling control of eye orientation in three dimensions. I. Role of muscle pulleys in determining saccadic trajectory. *J Neurophysiol* 79: 2653–2667, 1998.

RAYBOURN MS AND KELLER EL. Colliculoreticular organization in primate oculomotor system. *J Neurophysiol* 40: 861–878, 1977.

ROBINSON DA. Oculomotor unit behavior in the monkey. *J Neurophysiol* 33: 393–404, 1970.

ROBINSON DA. Eye movements evoked by collicular stimulation in the alert monkey. *Vision Res* 12: 1795–1808, 1972.

ROBINSON DA. Oculomotor control signals. In: *Basic Mechanisms of Ocular Motility and Their Clinical Implications*, edited by Bach-y-Rita P and Lennerstrand G. Oxford, UK: Pergamon, 1975, p. 337–374.

RUETE CGT. *Lehrbuch der Ophthalmologie fuer Aertze und Studirende* (2 vols.). Braunschweig, Germany: Vieweg, 1855.

SACHS L. *Applied Statistics: A Handbook of Techniques.* New York: Springer-Verlag, 1984.

SAUVAN XM. Early integration of retinal and extra-retinal information: recent results and hypotheses. *Rev Neurosci* 9: 291–299, 1998.

SAUVAN XM AND PETERHANS E. Integration of visual information and direction of gravity in prestriate cortex of the awake behaving monkey. *Supp Eur J Neurosci* 8: 75, 1995.

SCHERBERGER H, CABUNGCAL JH, HEPP K, SUZUKI Y, STRAUMANN D, AND HENN V. Pre-saccadic reticular burst neuron on-directions rotate with ocular counterroll in monkeys. *Soc Neurosci Abstr* 28: 60.5, 1998a.

SCHERBERGER H, HEPP K, SUZUKI Y, STRAUMANN D, AND HENN V. On-directions of pre-saccadic short-lead burst neurons rotate with ocular counterroll in monkeys (Abstract). *Eur J Neurosci* 10: 189, 1998b.

SCHNABOLK C AND RAPHAN T. Modeling three-dimensional velocity-to-position transformation in oculomotor control [published erratum appears in *J Neurophysiol* 1994 May;71(5): following table of contents]. *J Neurophysiol* 71: 623–638, 1994.

SPARKS DL. Conceptual issues related to the role of the superior colliculus in the control of gaze. *Curr Opin Neurobiol* 9: 698–707, 1999.

STRAUMANN D, ZEE DS, SOLOMON D, AND KRAMER PD. Validity of Listing's law during fixations, saccades, smooth pursuit eye movements, and blinks. *Exp Brain Res* 112: 135–146, 1996.

SUZUKI Y, KASE M, KATO H, AND FUKUSHIMA K. Stability of ocular counterrolling and Listing's plane during static roll-tilts. *Invest Ophthalmol Vis Sci* 38: 2103–2111, 1997.

SUZUKI Y, STRAUMANN D, SIMPSON JI, HEPP K, HESS BJM, AND HENN V. Three-dimensional extraocular motoneuron innervation in the rhesus monkey. I. Muscle rotation axes and on-directions during fixation. *Exp Brain Res* 126: 187–199, 1999.

TWEED D. Three-dimensional model of the human eye-head saccadic system. *J Neurophysiol* 77: 654–666, 1997.

TWEED D AND VILIS T. Implications of rotational kinematics for the oculomotor system in three dimensions. *J Neurophysiol* 58: 832–849, 1987.

TWEED D AND VILIS T. Geometric relations of eye position and velocity vectors during saccades. *Vision Res* 30: 111–127, 1990.

VAN OPSTAL AJ, HEPP K, HESS BJM, STRAUMANN D, AND HENN V. Two- rather than three-dimensional representation of saccades in monkey superior colliculus. *Science* 252: 1313–1315, 1991.

VILIS T, HEPP K, SCHWARZ U, AND HENN V. On the generation of vertical and torsional rapid eye movements in the monkey. *Exp Brain Res* 77: 1–11, 1989.

WURTZ RH. Visual receptive fields of striate cortex neurons in awake monkeys. *J Neurophysiol* 52: 727–742, 1969.